Journal of Hazardous Materials 188 (2011) 172–180

Contents lists available at ScienceDirect

Journal of Hazardous Materials

journal homepage: www.elsevier.com/locate/jhazmat

Enhanced photocatalytic activity of C–N-codoped TiO_2 films prepared via an organic-free approach

Qing Chi Xu [a], Diana V. Wellia [a], Shi Yan [b], Dai Wei Liao [b], Tuti Mariana Lim [c], Timothy Thatt Yang Tan [a,*]

[a] School of Chemical and Biomedical Engineering, Nanyang Technological University, 62 Nanyang Drive, Singapore 637459, Singapore
[b] Department of Chemistry, College of Chemistry and Chemical Engineering, Xiamen University, Xiamen 361005, People's Republic of China
[c] School of Life Sciences and Chemical Technology, Ngee Ann Polytechnic, Singapore, Singapore

ARTICLE INFO

Article history:
Received 6 November 2010
Received in revised form 1 January 2011
Accepted 21 January 2011
Available online 27 January 2011

Keywords:
TiO_2
Dopant
Carbon
Nitrogen
Visible light
Organic-free

ABSTRACT

An organic-free sol–gel method was developed to synthesize crack-free, high surface roughness and visible-light-active C–N-codoped TiO_2 films. These films were subsequently evaluated for its photodegradation efficient using stearic acid as the model pollutant compound. The current approach avoids the use of hazardous organic solvents and employs carbon black as the carbon source as well as a template to increase the surface roughness. The presence of carbon and nitrogen species in TiO_2 was studied and discussed. The concentrations of carbon and nitrogen dopants in the TiO_2 films were affected by calcination temperature and the concentration of carbon black. Optimal visible light photocatalytic activity was observed for C–N-codoped TiO_2 film at 10.0 wt.% C, which was more than double that of the N-doped TiO_2 film. The enhancement in visible light photocatalytic activities of the C–N-codoped TiO_2 films was attributed to the synergistic effects of carbon and nitrogen dopants, and high surface roughness of the prepared films.

1. Introduction

Among various types of photocatalysts, titanium dioxide (TiO_2) is the most widely investigated due to its attractive attributes of being low cost, non-toxicity and chemical stability [1–3]. TiO_2 films coated on glass slides have potential applications in self-cleaning [4], solar cells [5] and decontamination of hazardous pollutant and microbes [6]. However, pure anatase TiO_2 film can only be activated under UV light due to its wide band gap (3.2 eV). Efforts made to extend its optical absorption edge from UV to visible light region include doping with transition metals (Cr, Fe, Mn, and V) [7–10] and nonmetal atoms (N, S, and C) [11–14]. However, transition metals doped TiO_2 have been found to suffer from thermal instability and an increase of carrier-recombination centers, which could decrease photocatalytic efficiency [15,16]. Among all the nonmetal-doped TiO_2 photocatalysts, carbon doped TiO_2 and nitrogen doped TiO_2 are widely investigated both experimentally and theoretically [11,17,18]. According to the previous reports, three forms of carbon species have been detected in C-doped TiO_2: elemental carbon located within the tetrahedral and octahedral interstices in the anatase crystal, the carbonate species adsorbed on the surface and carbon atoms substituting atoms in the lattice of TiO_2 [19,20]. Similarly, there are different forms of nitrogen species in N-doped TiO_2 detected in previous works: nitrogen atoms substituting oxygen atoms in the lattice of TiO_2 and molecular chemisorbed nitrogen or NO_x or NH_3 [18,21].

More recently, codoped TiO_2 has attracted considerable interest, since it can result in a higher visible light photocatalytic activity compared with single element doped TiO_2. For example, S–N [22], F–N [23], B–N [24] and C–N [21,25–27] codoped TiO_2 powders were reported to significantly improve the photocatalytic efficiency under visible light illumination. In our previous work, we reported the preparation of visible-light-active C–N–F-codoped TiO_2 films, which exhibited much higher photocatalytic activities than single doped TiO_2 film under visible light illumination [14]. Noguchi et al. reported the preparation of C–N-codoped TiO_2 films by using a dc reactive magnetron sputtering method [28]. This method involves expensive equipment due to the requirement of a highly regulated environment, and may be difficult to scale up [29]. Among all the techniques for the preparation of TiO_2 or nonmetal-doped TiO_2 films, the sol–gel method is the most widely used method as it presents many advantages such as the use of very simple equipment, low capital investment, and the ability to control the microstructure and density of thin films. However, traditional sol–gel method usually involves the use of organic solvents which are considered as hazardous materials themselves. Yang et al. prepared C–N-codoped TiO_2 films by using dip-coating method and heating TiO_2 gel-films in an ionized N_2 gas [30]. Their method involves organic titanium precursor, organic solvents and large

* Corresponding author. Tel.: +65 63168829; fax: +65 67911761.
E-mail address: tytan@ntu.edu.sg (T.T.Y. Tan).

0304-3894/$ – see front matter © 2011 Elsevier B.V. All rights reserved.
doi:10.1016/j.jhazmat.2011.01.088

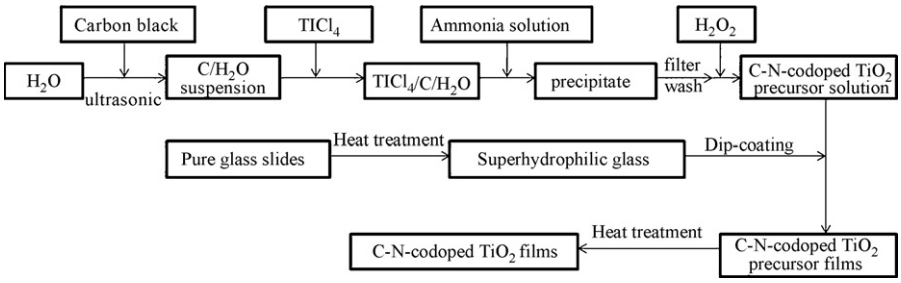

Fig. 1. Scheme of the preparation of C–N-codoped TiO_2 films from aqueous peroxotitanate solution.

amount of gas, which are potentially environmental pollutants and could be expensive.

Very few studies reported the use of organic-free aqueous peroxotitanate (PTA) solutions to prepare visible-light-active TiO_2 films [31–34], and no studies have reported the preparation of C–N-codoped TiO_2 films using PTA solutions as Ti source. Due to the high surface tension of water-based solution, aqueous peroxotitanate solution could not disperse uniformly on glass surfaces which often resulted in cracks in the TiO_2 films [31–34]. In our previous work, we reported a new method for the preparation of N-doped TiO_2 films by exploiting the superhydrophilicity of freshly calcined glass slides, and using aqueous peroxotitante solution as the Ti source and NH_3 in Ti complex as the nitrogen source [35]. The N-doped TiO_2 coated glass slides were transparent, crack-free, exhibited relative high photocatalytic activity under visible light illumination but consisted of a relatively flat surface structure. It is well known that the photocatalytic activity can be greatly enhanced by high surface area and porosity [36,37]. Addition of polymer template, such as PEG and PS, has been proven to be successful in the development of porous and high surface area TiO_2 film [38,39].

The current work reports an organic-free preparation and characterizations of C–N-codoped TiO_2 films with high surface roughness and high visible light photocatalytic activity. Ammonia in PTA solution was used as nitrogen source, while carbon black was chosen as the carbon source and surface roughness inducing agent. Stearic acid was selected as the model pollutant in the evaluation of the visible-light photocatalytic activity. The synergy of carbon and nitrogen dopants in enhancing visible light photocatalytic activity is discussed and a mechanism is proposed.

2. Experimental details

2.1. Reagents

Titanium (IV) chloride (purity > 99%) and ammonia solution (25%) were purchased from Merck. Carbon black and sodium hydroxide were purchased from Sigma. Hydrogen peroxide (30%) was purchased from AnalaR. The chemicals were used without further purification.

2.2. Preparation of C–N-codoped TiO_2 precursor

A modified method involving the use of aqueous peroxotitanate solution (PTA) was used to prepare the C–N-codoped TiO_2 [35]. In a typical synthesis, carbon black (5.0, 10 and 20 wt.% with respect to TiO_2) was dispersed in 300 ml distilled water and ultrasonically treated for 1 h. 3.6 ml of $TiCl_4$ was then added drop-wise into the carbon suspension solution in an ice bath under vigorous stirring. The pH of the solution was then adjusted to 10 by drop-wise addition of diluted ammonia solution (3.0 M). After stirring for 24 h, the obtained precipitate was filtered and washed thoroughly with distilled water repeatedly until no Cl^- was detected. Thereafter the precipitates were ultrasonically dispersed in 80 ml distilled water. H_2O_2 (28 ml) was added drop-wise into this mixture under continuous stirring. The theoretical concentration of TiO_2 in the resulting carbon–nitrogen-PTA solution (CN5-PTA, CN10-PTA and CN20-PTA respectively, according to the concentration of carbon black) was adjusted to 2.0 wt% for subsequent coating. Separate solutions of nitrogen-PTA (N-PTA, without carbon), carbon-PTA (C-PTA, 10 wt.% of carbon black with respect to TiO_2, ammonia solution was replaced by NaOH solution) and PTA (without carbon black and ammonia solution was replaced by NaOH solution) were also prepared.

For the TG-DTA measurement, the obtained N-PTA and CN10-PTA (10 wt.% C) solutions were heated at 100 °C to evaporate the solvent and dried in oven at 100 °C for 3 h. For XRD and BET measurements, the obtained yellow powder (N-PTA) and black powders (CN5-PTA, CN10-PTA and CN20-PTA) were further heated at 500 °C for 1 h to form NT-500, CNT5-500, CNT10-500 and CNT20-500 powders, respectively.

2.3. Preparation of C–N-codoped TiO_2 films

Glass slides were heated at 500 °C for 1 h with a heating speed of 10 °C/min, cooled down to room temperature and used within 0.5 h. CN10-PTA solution was coated on the superhydrophilic glass slides using a KSV Dip Coater at a withdrawal speed of 0.2 cm/s. The coated glass slides (CN10-PTA, 10 wt.% carbon black) were dried in vacuum at room temperature for 10 min and then calcined in air at a heating speed of 10 °C/min and kept at 450 °C, 500 °C and 550 °C for 1 h respectively. Finally the samples were cooled to room temperature. The obtained films were labeled as CNT10-450, CNT10-500 and CNT10-550 respectively, according to the calcination temperatures.

The C–N-codoped TiO_2 films with different concentrations of carbon black were prepared at 500 °C using CN5-PTA, CN10-PTA and CN20-PTA as dip-coating solution, and the obtained films were labeled as CNT5-500, CNT10-500 and CNT20-500 respectively in accordance to the original concentrations of carbon black. The scheme of the preparation of C–N-codoped TiO_2 films is illustrated in Fig. 1. N-TiO_2 film (NT-500), C-TiO_2 film (CT-500) and pure TiO_2 film (T-500) were also prepared by using N-PTA, C-PTA and PTA solutions as dip-coating solutions, respectively.

2.4. Characterization

X-ray diffraction analysis (XRD) was carried out using a Philips PW1010 X-ray diffractometer with Cu Kα radiation. XRD pattern was recorded with a scan step of 1° min^{-1} (2θ) in the range from 20° to 70°. Surface species of these samples were analyzed by Fourier Transform Infrared Spectroscopy (FTIR, Digilab FTS 3100). X-ray photoelectron spectroscopy (XPS) analysis was carried out with a PHI Quantum 2000 Scanning ESCA Micro-probe equipment (Physical Electronics, MN, USA) using monochromatic Al-Kα radiation. The X-ray beam diameter was 100 μm, and the pass energy was 29.35 eV for the sample. The binding energy was calibrated with

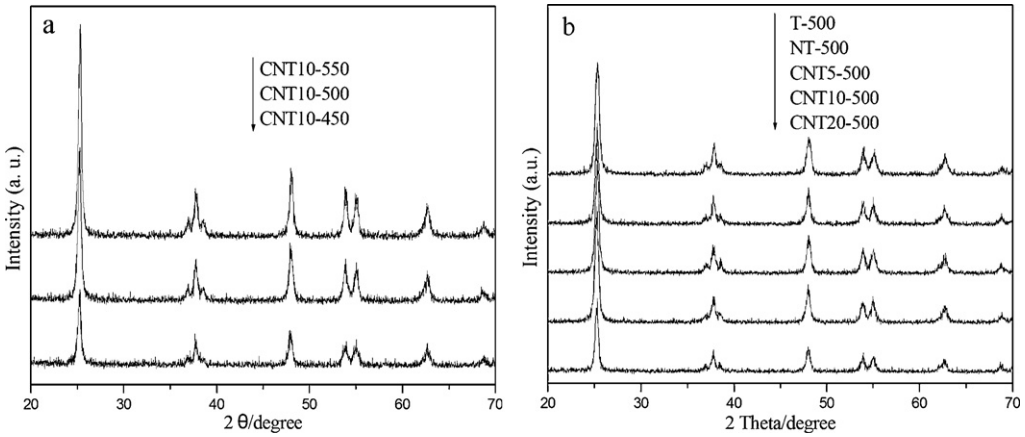

Fig. 2. XRD pattern of C–N-codoped TiO_2 prepared at (a) different calcination temperatures and (b) different carbon black concentrations.

respect to C (1s) at 284.6 eV. Surface morphologies of C–N-codoped TiO_2 films were evaluated by JEOL field emission electron microscope (FESEM) JSM-6700F. Surface roughness and morphologies of C–N-codoped TiO_2 film were evaluated by atomic force microscopy (AFM, MFP 3D). Nitrogen adsorption–desorption isotherms were measured at −196 °C on a Quantachrome AUTOSORB-6B static volumetric instrument. Prior to measurements, the samples were degassed at 250 °C for 5 h under high vacuum. The specific surface areas were calculated using the BET method [40]. UV–vis spectra of films were obtained using a UV–visible spectrophotometer (Shimadzu).

2.5. Photocatalytic activity tests

For the evaluation of photocatalytic activities of the N-doped TiO_2 and C–N-codoped TiO_2 films, one 300 W halogen lamp held at 20 cm from the sample with a 420 nm UV filter (JB420) was used as the visible light source. Photocatalytic activity measurements were performed using stearic acid as the model organic compound, spin-coated on the surface of the photocatalyst films. 200 μl of stearic acid–methanol solution (0.015 M) was dropped on the films, followed by 2 min of 1000 rpm [41]. The thickness of the coated stearic acid films on the photocatalysts was around 30–40 nm. The change in stearic acid layer thickness was monitored by measuring the infrared absorption spectrum with a FTIR instrument (Digilab FTS 3100). The absorbance at 2917 cm^{-1} was converted to a thickness on the basis of an earlier observation that an absorbance intensity of 0.01 corresponds to a thickness of 12.5 nm [41].

3. Results and discussion

The crystalline phase and particle size of the C–N-codoped TiO_2 prepared at different calcination temperatures were determined by XRD (Fig. 2a). The distinctive peaks at $2\theta = 25.3°$, 38.0°, 48.1°, 53.8°, 54.8° and 62.8° are attributed to the anatase TiO_2, which indicates that all the C–N-codoped TiO_2 films mainly consist of anatase phase. It is obvious that the intensity of CNT10-450 is lower compared to that of CNT10-500 and CNT10-550, which is due to lower amount of crystalline phase formed at lower temperature. The crystal sizes of CNT10-450, CNT10-500 and CNT10-550 were determined to be 16.5 nm, 17.2 nm and 20.5 nm, respectively, by Scherrer's equation. The crystal sizes increase with the increase of calcination temperatures, which is due to the aggregation of TiO_2 particles at high temperature.

The presence of carbon and nitrogen atoms in the CNT10-450, CNT10-500 and CNT10-550 films were revealed by XPS (Fig. 3a and b). The C 1s spectrum shows a single strong peak at 284.6 eV and a weak shoulder at around 288.5 eV, which are attributed to the presence of adventitious elemental carbon and C–O bond, respectively [42–44]. Generally, the C–O band at 288.5 eV has been considered as the formation of Ti–O–C bond due to the substitution of carbon for some of the lattice titanium atoms, though this peak may come from the surface functional group of carbon black [41–43]. The peak at around 281.0 eV of Ti–C bond was not observed in these samples, which suggests that carbon did not substitute for oxygen atom in the lattice of TiO_2 in the current system. It has been reported that the carbon doping states and species cannot be directly confirmed by only analyzing the XPS C 1s spectra [42,44]. Further analysis of the XPS Ti 2p spectra can help to investigate the carbon doping state, because carbon-doping can lead to the formation of oxygen vacancies and Ti^{3+} defects and result in a slight shift of the Ti 2p peaks toward the lower binding energy [42–44]. Fig. 3c shows a comparison of the Ti 2p peaks of the N-doped TiO_2 film (NTO-500) and C–N-codoped TiO_2 films. For the NTO-500 film, two XPS signals are observed at binding energies at around 458.7 eV and 464.5 eV, which are in good agreement with that of pure TiO_2 [43]. By comparing the Ti 2p peaks for all samples, the obvious red shift of C–N-codoped TiO_2 films toward the lower binding energy reveals the successful carbon-doping in these C–N-codoped TiO_2 films [42]. Moreover, the Ti 2p peaks of the CNT10-550 film are red shifted to the binding energies slightly lower than that of CNT10-450 and CNT10-500 films, which is probably due to the enhancement in carbon doping in TiO_2 at a higher temperature. The Ti^{3+} to Ti^{4+} ratios for the NT-500, CNT10-450, CNT10-500 and CNT10-550 films estimated from XPS curve fitting program are 0.1%, 4.0%, 10.5% and 11.3%, respectively. In Fig. 3a, the intensities of the peaks attributed to elemental carbon in the C–N-codoped TiO_2 films decrease with the increase of calcination temperature, which is due to the combustion of carbon black in the presence of air at higher temperature. The atomic percentages of carbon in the CNT10-450, CNT10-500 and CNT10-550 films are determined to be 42.51 at%, 28.59 at% and 26.27 at%, respectively. It should be noted that some of the carbon atoms in the C–N-codoped TiO_2 films are originated from the equipment itself.

So far, the carbon states and species in carbon-doped TiO_2 which are responsible for visible light photocatalytic activity have remained controversial. Khan et al. [12] and Irie et al. [45] reported that the band-gap narrowing of C-doped TiO_2 was caused by the shift of valence band edge to higher energy as a result of the substitutional carbon atoms in the lattice of TiO_2. Lee et al. [42] and Ren et al. [43] reported that the formation of Ti–O–C led to the enhancements of visible light absorption and photocatalytic activities. Yang et al. [46] and Lettmann et al. [47] reported that the

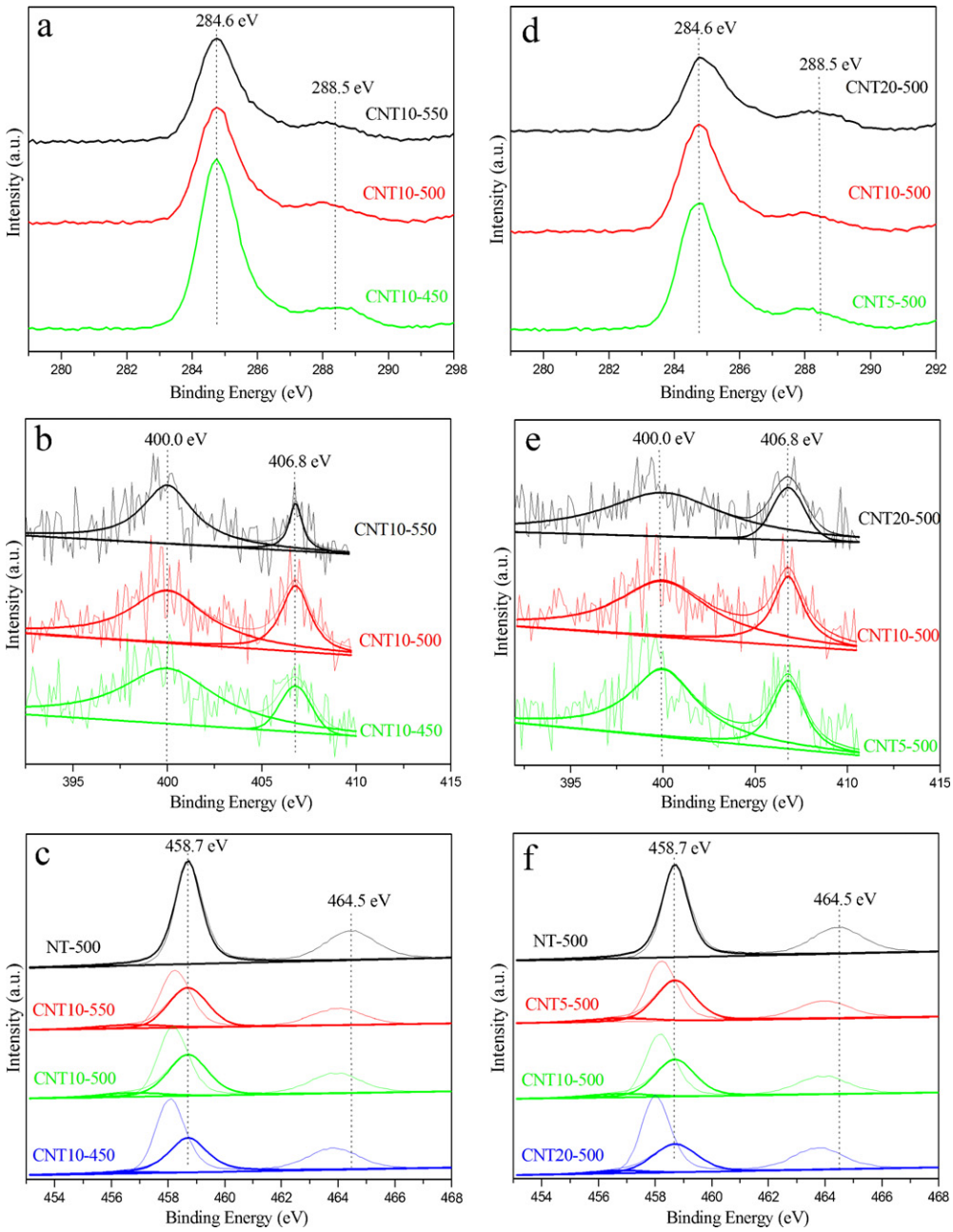

Fig. 3. XPS spectra of C–N-codoped TiO_2 films (a) C spectra; (b) N spectra; (c) Ti spectra at different temperature and (d) C spectra; (e) N spectra (f) Ti spectra at different carbon black concentrations.

elemental carbon incorporated interstitially in C-doped TiO_2 was responsible for the visible light absorption up to 600 nm. Sakthivel and Kisch [17] and Ohno et al. [48] found that the absorption edge of TiO_2 was largely shifted to 700 nm by carbonate species absorbed on the TiO_2 surface. In the current work, our XPS data strongly suggest the presence of carbon doped into the TiO_2 material, and hence resulting in enhanced absorption and hence visible-light photocatalytic activity.

For the N 1s spectrum, two peaks appear at 400.0 eV and 406.8 eV. The peak at 406.8 eV is generally considered as the evidence for the presence of nitrate species [49]. The XPS signal of nitrogen at around 400.0 eV has also been a subject of controversy in the identification of nitrogen species in the study of N-doped TiO_2. Many reports had suggested that the signal at 400.0 eV was attributed to NO_x species adsorbed on crystallite surface [49]. Sakthivel et al. [50] and Navio et al. [51] reported that the signal at around 400.0 eV was attributed to the presence of hyponitrite. Qiu et al. assigned the signal at 400.0 eV to the nitrogen incorporated into the TiO_2 lattice [52]. However, they unanimously reported that the peak at 400.0 eV was critical for a visible light response. The atomic percentages of nitrogen in the CNT10-450, CNT10-500 and CNT10-550 films were determined to 0.41 at%, 0.32 at% and 0.26 at%, respectively. The atomic percentages of nitrogen decreased with the increase of calcination temperature. According to previous reports, a higher temperature resulted in lower atomic percentage of nitrogen doped in TiO_2, which may be attributed to desorption of nitrogen species on TiO_2 at high temperature [26,53–55]. The accuracy of nitrogen quantification can vary from 5% to about 30% depending on parameters such as signal to noise ratio and peak intensities [56]. In the current work, the major peaks are reported and thus it is reasonable to assume the accuracy to be around 90–95%. We estimate the error to be ±0.04 at.%, ±0.03 at.%

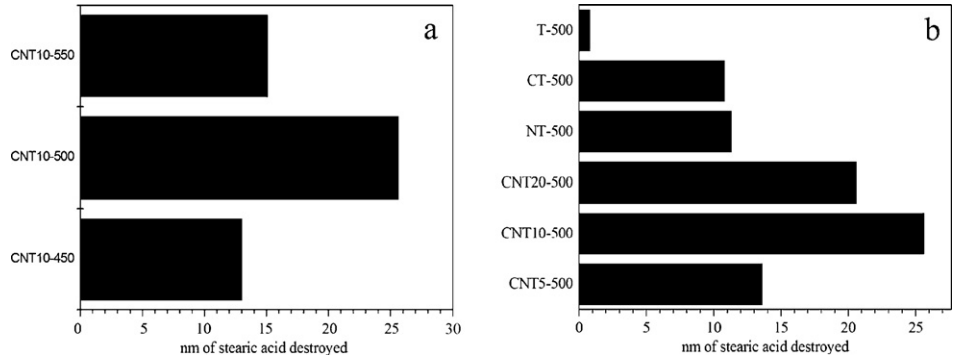

Fig. 4. Photocatalytic activities of C–N-codoped TiO_2 films prepared at (a) different calcination temperatures and (b) different carbon black concentrations.

and ±0.03 at.% for the CNT10-450, CNT10-500 and CNT10-550 films, respectively.

In order to investigate the optimal calcination temperature, the photocatalytic activities of CNT10-450, CNT10-500 and CNT10-550 films were evaluated by monitoring the degradation of stearic acid under visible light illumination (Fig. 4a). The photocatalytic activities were evaluated based on the thickness (in nm) of stearic acid degraded after 24 h of visible light illumination [57]. The CNT10-500 film exhibits the highest photocatalytic activity, with 25.6 nm of stearic acid degraded. The relative lower photocatalytic activity of the CNT10-450 film probably can be attributed to its lower crystallinity. For the CNT10-550 film, the increase of nanoparticle size and the decrease of carbon and nitrogen concentrations could be responsible for the lower photocatalytic activity, compared with that of the CNT10-500 film. Based on the above results, 500 °C is considered to be the optimal calcination temperature for the preparation of C–N-codoped TiO_2 films.

To further optimize the photocatalytic film, different concentrations of carbon black were used to prepare C–N-codoped TiO_2 films. The crystalline phase and particle size of T-500, NT-500, CNT5-500, CNT10-500 and CNT20-500 were determined by XRD (Fig. 2b). The distinctive peaks at $2\theta = 25.3°$, 38.0°, 48.1°, 53.8°, 54.8° and 62.8° are attributed to anatase TiO_2. Compared to the pure TiO_2 (T-500), no shift of the peak position is observed for NT-500, CNT5-500, CNT10-500 and CNT20-500, which probably because C/N do not substitute the atoms in TiO_2 lattice or the concentration of C/N substituted in TiO_2 lattice is low. The crystal sizes of CNT5-500, CNT10-500 and CNT20-500 were determined to be 17.5 nm, 17.2 nm and 17.0 nm respectively using Scherrer's equation. Wang et al. prepared nanocrystalline TiO_2/activated-carbon composite catalysts for the degradation of chromotrope 2R [58]. They found that the combustion of carbon during calcinations resulted in a higher temperature inside the composite catalysts and the increase of TiO_2 particle size [58]. However, Yu et al. reported that carbon doped into TiO_2 increased steric hindrance for grain growth and decreased TiO_2 particle size [59]. In our case, the particle sizes of C–N-codoped TiO_2 films were not significantly affected by the concentration of carbon black.

FTIR analysis of CN5-PTA, CN10-PTA, CN20-PTA, N-PTA and PTA films before (Fig. 5a) and after 500 °C calcination (Fig. 5b) was performed. In Fig. 5a, the absorption bands at 900 cm^{-1} are attributed to the stretching vibrations of peroxo band (O–O) [34]. The bands at 1620 cm^{-1} and the wide bands at 3100–3700 cm^{-1} are resultant from O–H bending of adsorbed water molecules. The bands at 1400 cm^{-1} are assigned to the stretching vibrations of the N–H bonds in NH_3, which evidences the presence of NH_3 in Ti complex [35]. The NH_3 in the Ti complex is regarded as a nitrogen source for the N-doped TiO_2 [35,49]. The band at 1400 cm^{-1} is not observed for PTA. Fig. 5b shows the FTIR of these samples after calcination. It is obvious that the O–O bands at 900 cm^{-1} and the N–H bands at 1400 cm^{-1} disappear, which evidences the decomposition of peroxotitanate and NH_3. The signals in the range 400–1250 cm^{-1} are characteristic of the formation of an O–Ti–O lattice [57]. There are no obvious stretching bands attributed to the NO_x species, which is probably due to the low atomic percentage of nitrogen doping in TiO_2.

To elucidate the effect of carbon on CN-PTA, N-PTA was used for photocatalytic performance comparison. Typical TG-DTA patterns of the as-synthesized N-PTA and CN-PTA (10 wt.% C) powders are shown in Fig. 6. At temperatures near 100 °C, an endothermic peak is observed, which is resulted from the evaporation of adsorbed water. The exothermic peaks near 250 °C are attributed to the decomposition of peroxo group in peroxotitanate [60]. The broad exothermic peaks at 350–370 °C correspond to the crystallization of amorphous TiO_2 to anatase TiO_2 [61]. The weight loss at the temperature lower than 350 °C is mainly attributed to the

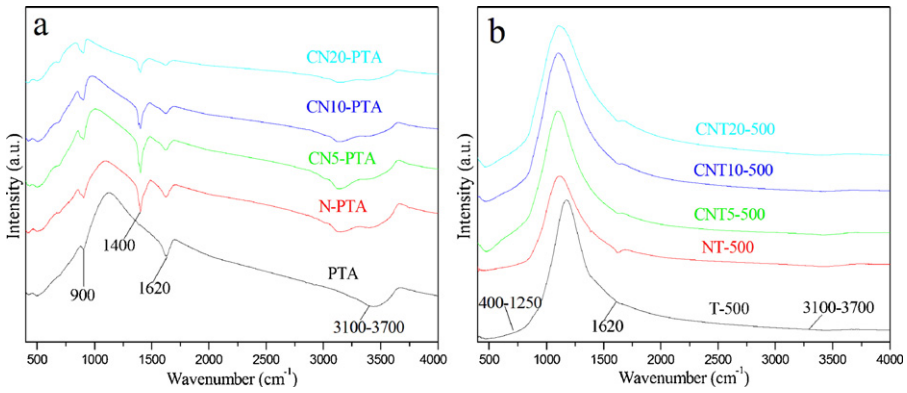

Fig. 5. FTIR spectra of the CN5-PTA, CN10-PTA, CN20-PTA, N-PTA and PTA (a) before and (b) after calcination at 500 °C.

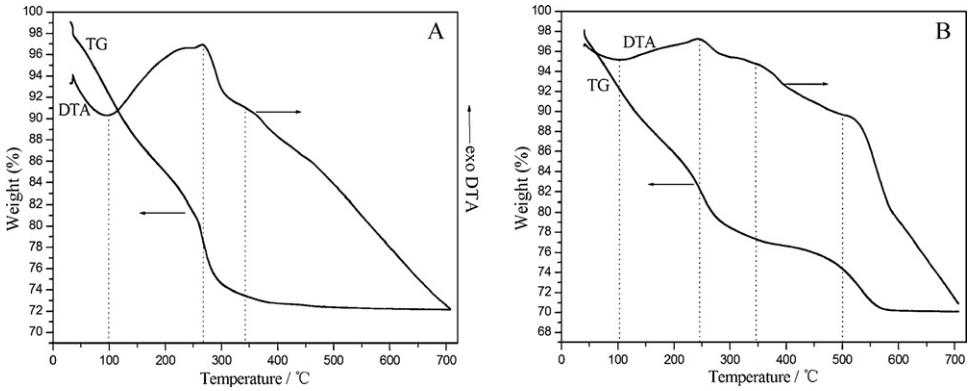

Fig. 6. TG-DTA patterns in air of the (a) N-PTA and (b) C–N-PTA composites.

removal of adsorbed water and the decomposition of peroxo group. For the N-PTA (Fig. 6a), there is no further obvious weight loss in the range of 350–700 °C. However, for the CN-PTA, there is approximately 6 wt.% of weight loss in the range of 400–550 °C and a big exothermic peak near 500 °C, which is attributed to the combustion of carbon. The combustion of carbon during calcinations resulted in a higher temperature inside the catalysts, which is consistent with the result reported by Wang et al. [58].

The presences of carbon, nitrogen and Ti atoms in the CNT5-500, CNT10-500 and CNT20-500 films were also revealed by XPS (Fig. 3d–f). Similarly, the C 1s spectrum shows a single strong peak at 284.6 eV and a weak shoulder at around 288.5 eV, and the N 1s spectrum shows two peaks at 400.0 eV and 406.8 eV. The atomic percentages of nitrogen in the CNT5-500, CNT10-500 and CNT20-500 films were determined to be 0.39 at.%, 0.32 at.% and 0.15 at.% respectively. The atomic percentages of nitrogen decrease with the increase of the concentration of carbon black. This could be due to the combustion of carbon black, which releases high heat energy and increases the temperature of the C–N-codoped TiO_2 films [58]. Higher initial carbon content implies a greater amount of carbon to be burnt at 500 °C, which result in a higher inner temperature inside the composite catalysts during calcination process, and thus decrease the atomic percentage of nitrogen in TiO_2 [26,53–55]. A comparison of the Ti 2p peaks of the NTO-500 film and CNT5-500, CNT10-500 and CNT20-500 films is shown in Fig. 3f. An obvious red shift of the CNT5-500, CNT10-500 and CNT20-500 films toward the lower binding energy is observed, which may suggest successful carbon-doping in these C–N-codoped TiO_2 films [42]. The Ti^{3+} to Ti^{4+} ratios for the NT-500, CNT5-500, CNT10-500 and CNT20-550 films estimated from XPS curve fitting are 0.1%, 10.3%, 10.5% and 9.2%, respectively.

The morphologies of the NT-500, CNT5-500, CNT10-500 and CNT20-500 films were further investigated by using FESEM (Fig. 7). All the films are uniform and crack-free. The surface structure of NT-500 is very flat. However, with the increase of the concentration of carbon black, the surface roughness increases. Fig. 8

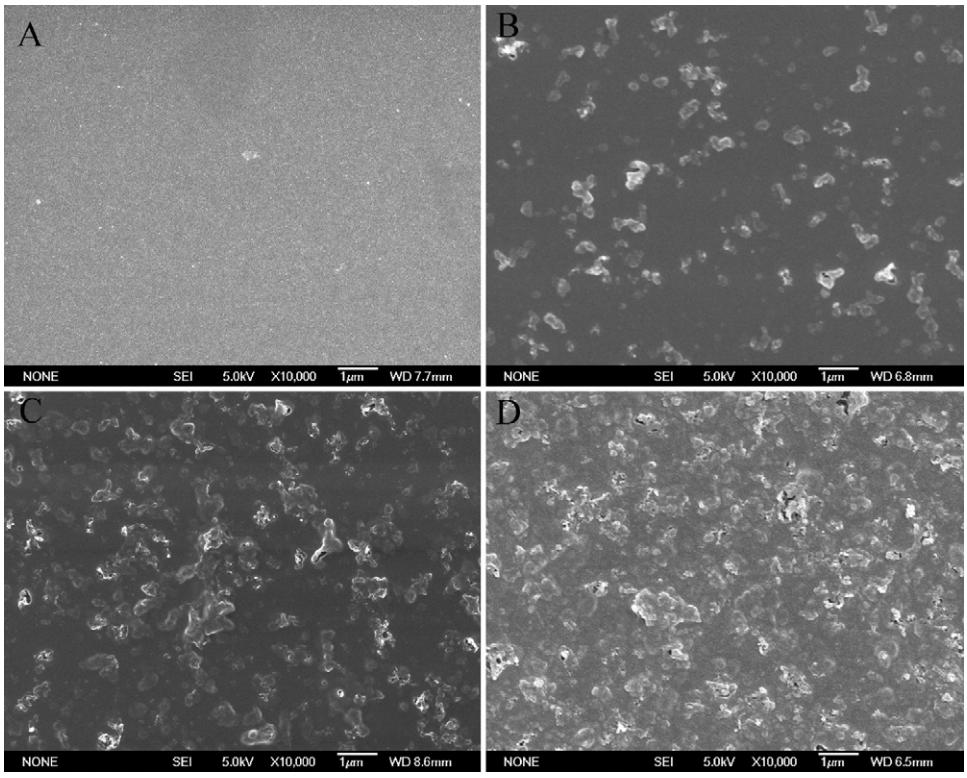

Fig. 7. FESEM images of (a) NT-500 film; (b) CNT5-500 film; (c) CNT10-500 film; (d) CNT20-500 film.

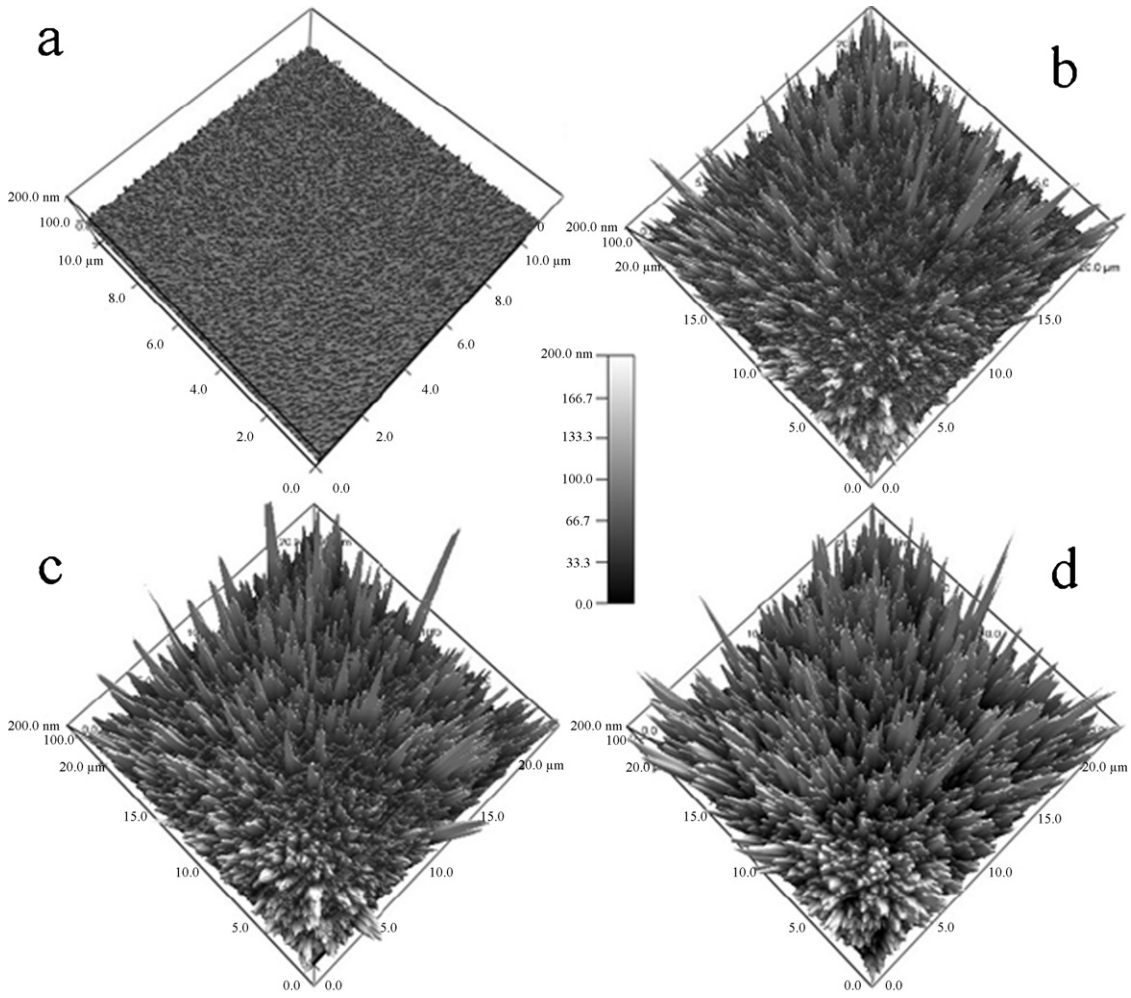

Fig. 8. AFM images of (a) NT-500 film; (b) CNT5-500 film; (c) CNT10-500 film; (d) CNT20-500 film.

displays the AFM 3D images of the NT-500, CNT5-500, CNT10-500 and CNT20-500 films. It further confirms that the addition of carbon black and calcination at 500 °C leads to the increases of surface roughness. The surface roughness of the NT-500, CNT5-500, CNT10-500 and CNT20-500 films are 3.2 nm, 35.6 nm, 48.8 nm and 61.8 nm, respectively, as determined by AFM. BET analysis of the NT-500, CNT5-500, CNT10-500 and CNT20-500 powder samples were determined to be 45.3, 53.6, 58.8 and 61.5 m^2/g respectively, indicating an increase in surface area and surface roughness with the increase of carbon black concentration. Yang et al. [21] reported that organic compounds were pre-adsorbed on the surface of the semiconductor particles to effectively utilize the photoexcitation, thus higher surface area can provide more surface active sites for the adsorption of organic compound and exhibit higher photocatalytic efficiency. Along with the function as a dopant, the carbon also increases the surface area, which may provide much more possibly accessible active sites, thus enhancing the photocatalytic activity.

The optical absorption spectra of the C–N-codoped TiO_2 films are shown in Fig. 9. All the C–N-codoped TiO_2 films exhibit absorption in the visible light region. The absorption intensities of C–N-codoped TiO_2 films in the visible region are higher than that of the NT-500 and T-500 films, due to the synergistic effects of carbon and nitrogen doping [21]. The absorption edges of the T-500 and NT-500 films are around 380 nm. There is no obvious red shift of the NT-500 film is observed compared with T-500 film, which is probably due to the fact that the doping state of nitrogen in TiO_2 is NO_x species adsorbed on crystallite surface and nitrogen does not substitute for oxygen in TiO_2 lattice. The absorption edges of these C–N-codoped films slightly shifts toward longer wavelengths of 390–393 nm, which further confirms the successful carbon-doping in these C–N-codoped films. The presence of both nitrogen and car-

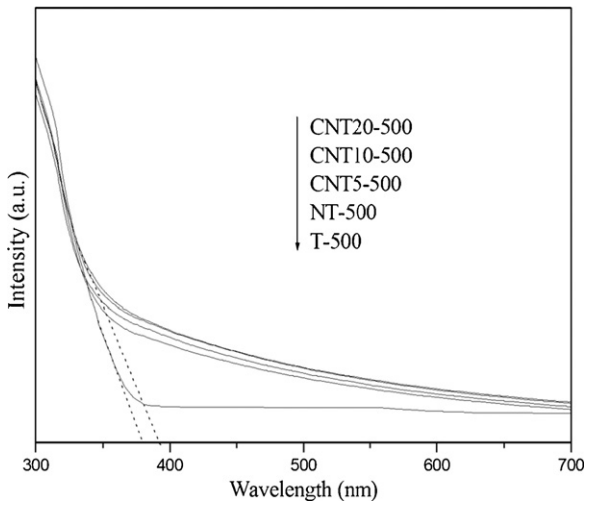

Fig. 9. UV–visible diffuse reflectance spectra of C–N-codoped TiO_2 films prepared at different carbon black concentration.

bon species in TiO_2 has evidently enhanced visible light absorption. The absorption intensities of C–N-codoped TiO_2 films in the visible region increase with the increase of the concentration of carbon black. However, the absorption intensity of CNT20-500 was only slightly enhanced in the visible light region compared with that of CNT10-500, even thought the concentration of carbon doping in CNT20-500 was higher than that of CNT10-500. This may due to the fact that the atomic percentage of nitrogen doping in CNT20-500 (0.15 at.%) is lower than that of CNT10-500 (0.32 at.%).

The photocatalytic activities of the NT-500, CNT5-500, CNT10-500 and CNT20-500 films under visible light illumination were evaluated (Fig. 4b). With an increase in carbon dopant concentration and surface roughness, the photocatalytic activities of C–N-codoped TiO_2 films was optimal at 10.0 wt.% C. The photocatalytic activity of CNT20-500 film was lower than that of CNT10-500 film, which may due to the decrease of nitrogen dopant. It was found that 25.6 nm of stearic acid was degraded on the CNT10-500 film, which was more than double that of NT-500 film. To identify the synergistic effects of carbon and nitrogen dopants, the photocatalytic activities of CT-500 and T-500 films were measured for comparison. As shown in Fig. 4b, the photocatalytic activities of CT-500 and T-500 films are 10.8 nm and 0.8 nm in thickness of stearic acid layer degraded respectively, which are much lower than that of the CNT10-500 film. It should also be mentioned that no obvious decrease in stearic acid layer thickness (<0.5 nm) was observed for uncoated glass slides under visible light illumination. Herein, the high photocatalytic activities of C–N-codoped TiO_2 films are attributed to the high surface area and the synergistic effects of carbon and nitrogen dopants [21].

A mechanism on photogenerated charge transfer attributed to the synergy of carbon and nitrogen dopants in TiO_2 under visible light illumination is proposed. Carbon-doping in TiO_2 may lead to the formation of impurity level above the valence band of TiO_2. Under visible light illumination, the photoelectron can be excited to the conduction band of TiO_2 [46]. Electrons can also be excited from surface states energy level (from the nitrogen surface species) to the conduction band of anatase TiO_2 under visible light illumination [62]. Subsequently, the photogenerated electrons are directly captured by the adsorbed O_2 molecules on the surface of C–N-codoped TiO_2 to form O_2^-, which is capable of degrading organic compounds [46,47]. In addition, the photogenerated holes at both the impurity level and surface states can directly oxidize organic compounds, or be trapped by surface hydroxyl groups to form active hydroxyl radicals ($OH^\bullet$). For the current C–N-codoped TiO_2 films, electron–hole pairs can be generated simultaneously by both routes. Hence, co-doping the current TiO_2 films with Ti–O–C band and nitrogen surface species may lead to an increase of photogenerated electrons and holes, compared with pure TiO_2 and single N-doped TiO_2 films, thus leading to an increase of visible light photocatalytic activity as observed in the current work.

4. Conclusion

We have developed an organic-free method for the preparation of C–N-codoped TiO_2 films by using aqueous peroxotitanate solution as the Ti source, NH_3 in Ti complex as the nitrogen source and carbon black as carbon source. The C–N-codoped TiO_2 films were uniform, crack-free and had high surface roughness. All the C–N-codoped TiO_2 films exhibited photocatalytic activities under visible light illumination. The photocatalytic activity of CNT10-500 film (10 wt% C) was found to be optimal and more than double that of NT-500 film under the same visible light illumination. The high photocatalytic activities of C–N-codoped TiO_2 films are attributed to the high surface area and the synergistic effects of carbon and nitrogen dopants.

Acknowledgement

Financial support from Nanyang Technological University AcRF Tier 1 RG29/07 is gratefully acknowledged.

References

[1] Y. Kuroda, T. Mori, K. Yagi, N. Makihata, Y. Kawahara, M. Nagao, S. Kittaka, Langmuir 21 (2005) 8026.
[2] A. Fujishima, K. Honda, Nature 238 (1972) 37.
[3] O. Khaselev, J.A. Turner, Science 280 (1998) 425.
[4] X. Feng, J. Zhai, L. Jiang, Angew. Chem. Int. Ed. 44 (2005) 5115.
[5] A. Mishira, M.K.R. Fischer, P. Bäuerle, Angew. Chem. Int. Ed. 48 (2009) 2474.
[6] T. Kawahara, Y. Konishi, H. Tada, N. Tohge, J. Nishii, S. Ito, Angew. Chem. Int. Ed. 41 (2002) 2811.
[7] S. Klosek, D. Raftery, J. Phys. Chem. B 105 (2001) 2815.
[8] M. Anpo, M. Takeuchi, J. Catal. 216 (2003) 505.
[9] A.K. Ghosh, H.P. Maruska, J. Electrochem. Soc. 124 (1977) 1516.
[10] W.Y. Choi, A. Termin, M.R. Hoffmann, J. Phys. Chem. 98 (1994) 13669.
[11] R. Asashi, T. Morikawa, T. Ohwaki, K. Aoki, Y. Taga, Science 293 (2001) 269.
[12] S.U.M. Khan, M. Al-shahry, W.B. Ingler, Science 297 (2002) 2243.
[13] T. Umebayashi, T. Yamaki, H. Itoh, K. Asai, Appl. Phys. Lett. 81 (2002) 454.
[14] Q.C. Xu, D.V. Wellia, M.A. Sk, K.H. Lim, J.S.C. Loo, D.W. Liao, R. Amal, T.T.Y. Tan, J. Photochem. Photobiol. A: Chem. 210 (2010) 181.
[15] Y. Sakata, T. Yamamoto, H. Gunji, H. Imamura, S. Tsuchiya, Chem. Lett. 2 (1998) 131.
[16] M. Iwasaki, M. Hara, H. Kawada, H. Tada, S. Ito, J. Colloid Interface Sci. 224 (2000) 202.
[17] S. Sakthivel, H. Kisch, Angew. Chem. Int. Ed. 42 (2003) 4908.
[18] H. Irie, Y. Watanabe, K. Hashimoto, J. Phys. Chem. B 107 (2003) 5483.
[19] X. Wang, S. Meng, X. Zhang, H. Wang, W. Zhong, Q. Du, Chem. Phys. Lett. 444 (2007) 292.
[20] Z. Shi, X. Ye, K. Liang, S. Gu, F. Pan, J. Mater. Sci. 22 (2003) 1255.
[21] X. Yang, C. Cao, L. Erickson, K. Hohn, R. Maghirang, K. Klabunde, J. Catal. 260 (2008) 128.
[22] J.H. Xu, J. Li, W.L. Dai, Y. Cao, H. Li, K. Fan, Appl. Catal. B: Environ. 79 (2008) 72.
[23] D. Li, H. Haneda, S. Hishita, N. Ohashi, Chem. Mater. 17 (2005) 2588.
[24] G. Liu, Y. Zhao, C. Sun, F. Li, G.Q. Lu, H.M. Cheng, Angew. Chem. Int. Ed. 47 (2008) 4516.
[25] Y. Ao, J. Xu, D. Fu, C. Yuan, Micropor. Mesopor. Mater. 118 (2009) 382.
[26] D. Chen, Z. Jiang, J. Geng, Q. Wang, D. Yang, Ind. Eng. Chem. Res. 46 (2007) 2741.
[27] Y. Cong, F. Chen, J. Zhang, M. Anpo, Chem. Lett. 35 (2006) 800.
[28] D. Noguchi, Y. Kawamat, T. Nagatomo, J. Electrochem. Soc. 152 (2005) 124.
[29] Y.F. Gao, Y. Masuda, Z. Peng, T. Yonezawa, K. Koumoto, J. Mater. Chem. 13 (2003) 608.
[30] J. Yang, H. Bai, Q. Jiang, J. Lian, Thin Solid Films 516 (2008) 1736.
[31] L. Ge, M.X. Xu, M. Sun, H.B. Fang, J. Sol–Gel Sci. Technol. 38 (2006) 47.
[32] Y.F. Gao, Y. Masuda, K. Koumoto, Langmuir 20 (2004) 3188.
[33] Y.F. Gao, Y. Masuda, K. Koumoto, Chem. Mater. 16 (2004) 1062.
[34] Z.F. Yuan, B. Li, J.L. Zhang, C. Xu, J.J. Ke, J. Sol–Gel Sci. Technol. 39 (2006) 219.
[35] Q.C. Xu, D.V. Wellia, R. Amal, D.W. Liao, J.S.C. Loo, T.T.Y. Tan, Nanoscale 2 (2010) 1122.
[36] S.S. Soni, M.J. Henderson, J.-F. Bardeau, A. Gibaud, Adv. Mater. 20 (2008) 1493.
[37] L.-W. Zhang, Y.-J. Wang, H.-Y. Cheng, W.-Q. Yao, Y.-F. Zhu, Adv. Mater. 21 (2009) 1286.
[38] X.X. Liu, Z.G. Jin, S.J. Bu, T. Yin, J. Sol–Gel Sci. Technol. 36 (2005) 103.
[39] Z.F. Liu, Z.G. Jin, X.X. Liu, Y.N. Fu, G.Q. Liu, J. Sol–Gel Sci. Technol. 38 (2006) 73.
[40] S. Brunauer, P.H. Emmett, E. Teller, J. Am. Chem. Soc. 60 (1938) 309–319.
[41] V. Pore, M. Ritala, M. Leskela, S. Areva, M. Jarn, J. Jarnstrom, J. Mater. Chem. 17 (2007) 1361.
[42] Y.-F. Lee, K.-H. Chang, C.-C. Hu, K.-M. Lin, J. Mater. Chem. 20 (2010) 5682.
[43] W. Ren, Z. Ai, F. Jia, L. Zhang, X. Fan, Z. Zou, Appl. Catal. B: Environ. 69 (2007) 138.
[44] E.M. Rockafellow, X. Fang, B.G. Trewyn, K. Schmidt-Rohr, W.S. Jenks, Chem. Mater. 21 (2009) 1187.
[45] H. Irie, Y. Watanabe, K. Hashimoto, Chem. Lett. 32 (2003) 772.
[46] X. Yang, C. Cao, K. Hohn, L. Erickson, R. Maghirang, D. Hamal, K. Klabunde, J. Catal. 252 (2007) 296.
[47] C. Lettmann, K. Hindenbrand, H. Kisch, W. Macyk, W.F. Maier, Appl. Catal. B: Environ. 32 (2001) 215.
[48] T. Ohno, T. Tsubota, K. Nishijima, Z. Miyamoto, Chem. Lett. 33 (2004) 750.
[49] H. Sun, Y. Bai, H. Liu, W. Jin, N. Xu, G. Chen, B. Xu, J. Phys. Chem. C 112 (2008) 13304.
[50] S. Sakthivel, M. Janczarek, H. Kisch, J. Phys. Chem. B 108 (2004) 19384.
[51] J.A. Navio, C. Cerrillos, C. Real, Surf. Interface Anal. 24 (1996) 355.
[52] X. Qiu, Y. Zhao, C. Burda, Adv. Mater. 19 (2007) 3995.
[53] S. Sato, Chem. Phys. Lett. 123 (1986) 126.
[54] S. Sato, R. Nakamura, S. Abe, Appl. Catal. A: Gen. 284 (2005) 131.
[55] A.V. Vorontsov, A.A. Altynnikov, E.N. Savinov, E.N. Kurkin, J. Photochem. Photobiol. A: Chem. 144 (2001) 193.
[56] C. Brundle Richard, E.A. Charles Jr., S. Wilson, Encyclopedia of Material Characterization, Butterworth-Heinemann, 1992.

[57] X. Chen, Y. Lou, A.C.S. Samia, C. Burda, J.L. Gole, Adv. Funct. Mater. 15 (2005) 41.
[58] W. Wang, C.G. Silva, J.L. Faria, Appl. Catal. B: Environ. 70 (2007) 470.
[59] G. Yu, Z. Chen, Z. Zhang, P. Zhang, Z. Jiang, Catal. Today 90 (2004) 305.
[60] H. Ichinose, M. Terasaki, H. Katsuki, J. Ceram. Soc. Jpn. 104 (1996) 715.
[61] Y.B. Ryu, W.Y. Jung, M.S. Lee, E.D. Jeong, H.G. Kim, S.-S. Park, G.-D. Lee, S.-S. Hong, React. Kinet. Catal. Lett. 93 (2008) 333.
[62] S.-H. Lee, E. Yamasue, K.N. Ishihara, H. Okumura, Appl. Catal. B: Environ. 93 (2010) 217.